LBL-15465
Preprint c.2

# Lawrence Berkeley Laboratory
UNIVERSITY OF CALIFORNIA

## Materials & Molecular Research Division

RECEIVED
LAWRENCE
BERKELEY LABORATORY
FEB 18 1983
LIBRARY AND
DOCUMENTS SECTION

To be submitted for publication

# THE DISTRIBUTION IN SPACE AND TIME OF THE HEAT OF REACTION DURING OXIDATION OF ZIRCALOY AND ITS EFFECT ON CORROSION KINETICS

Donald R. Olander

January 1983

TWO-WEEK LOAN COPY
This is a Library Circulating Copy which may be borrowed for two weeks. For a personal retention copy, call Tech. Info. Division, Ext. 6782.

Prepared for the U.S. Department of Energy under Contract DE-AC03-76SF00098

LBL-15465 c.2

## DISCLAIMER

This document was prepared as an account of work sponsored by the United States Government. While this document is believed to contain correct information, neither the United States Government nor any agency thereof, nor the Regents of the University of California, nor any of their employees, makes any warranty, express or implied, or assumes any legal responsibility for the accuracy, completeness, or usefulness of any information, apparatus, product, or process disclosed, or represents that its use would not infringe privately owned rights. Reference herein to any specific commercial product, process, or service by its trade name, trademark, manufacturer, or otherwise, does not necessarily constitute or imply its endorsement, recommendation, or favoring by the United States Government or any agency thereof, or the Regents of the University of California. The views and opinions of authors expressed herein do not necessarily state or reflect those of the United States Government or any agency thereof or the Regents of the University of California.

LBL - 15465

# The Distribution in Space and Time of the Heat of Reaction during Oxidation of Zircaloy and its Effect on Corrosion Kinetics

Donald R. Olander

Materials and Molecular Research
Division of Lawrence Berkeley
Laboratory and the
Department of Nuclear Engineering
University of California
Berkeley, California 94720

This work was supported by the Director, Office of Energy Research, Office of Basic Energy Sciences, Materials Sciences Division of the U.S. Department of Energy under contract # DE-AC03-76SF00098.

## ABSTRACT

Partitioning of the heat of combusion of zirconium during Zircaloy oxidation between the gas-oxide and oxide-metal interfaces was determined. The spatial distribution of the heat release is very sensitive to the poorly known partial molar enthalpy of oxygen dissolution in $ZrO_2$. This uncertainty is of minor consequence in the thermal analysis, however because temperature gradients in the specimen due to the heat released by oxidation are very small. The temperature is mainly a function of time only. A simple lumped-capacity thermal analysis suffices to describe the temperature transient initiated by the corrosion process. A method of coupling the temperature rise due to the heat release to the corrosion kinetics is developed and applied to laboratory testing of individual slab specimens cooled by radiation.

# I INTRODUCTION

Although oxidation of a metal is accompanied by considerable release of heat, most analyses of this process assume that the temperature of the reacting solid is specified by the external environment. However, when external heat removal rates are low, the heat of combustion can be a significant heat source, as was dramatically illustrated by the accident at the Three Mile Island nuclear reactor. In this case, the energy released by oxidation of the Zircaloy cladding exceeded that provided by decay of the fission products in the fuel contained by the cladding tubes. In laboratory experiments in which a specimen is held in a furnace or heated by induction or by resistance, rapid oxidation can provide a heat source comparable in magnitude to that supplied by the applied heating method. The localized nature of the heat release by oxidation can cause temperature nonuniformities in the reacting metal which must be understood quantitatively if the corrosion process is to be properly modeled.

In this work, oxidation of zirconium is analyzed with reaction heating considered. Zirconium oxidizes by formation of a coherent oxide scale through which oxygen is transported by ionic diffusion from the gas to the metal. At the oxide-metal boundary, the incoming oxygen either converts some of the metal to oxide or dissolves into the metal and continues to penetrate by interstitial diffusion. The heat of reaction is released at both the gas-oxide and the oxide-metal boundaries, and possibly within the bulk phases as well. In oxidation of zirconium at high temperature, the metal phase consists of α-zirconium and β-zirconium components. The difference in the heat relased by dissolving oxygen in these two phases is not known, but is probably small. For the purpose of the thermal analysis, the distinction between α-Zr and β-Zr is not important.

# II COMPONENTS OF THE HEAT OF COMBUSTION OF ZIRCONIUM

The heat of formation of $ZrO_2$, $\Delta H^o_{fZrO_2}$ , is the enthalpy change of the reaction:

$$Zr + O_2(g) = ZrO_2 \qquad (1)$$

where the zirconium reactant is initially free of oxygen and the oxide product is stoichiometric (i.e, with an O/Zr ratio of 2). With reference to the isotherm on the phase diagram of Fig. 1, the heat of formation corresponds to the difference in enthalpy between points a and d. This difference can be divided into three parts.

a - b : Addition of ½ y moles of gaseous, gaseous oxygen to 1 g atom of pure zirconium to produce the saturated metal (O/Zr = y). This reaction is written as:

$$O_2(g) = 2O \text{ (sol'n in metal)} \qquad (2)$$

and the heat release follows from the definition

$$\overline{H}_1 = (\partial H/\partial N_1)_{N_2}$$

by integrating at constant $N_2$. For oxygen in Zr, this yields:

$$Q_{a-b} = -\tfrac{1}{2}\int_0^y \overline{\Delta H}_M dy' \simeq -\tfrac{1}{2}\ \overline{\Delta H}_M y \qquad (3)$$

where $\overline{\Delta H}_M$ is the partial molar enthalpy of oxygen in the metal. This quantity is assumed to be independent of composition, and, as explained earlier, to be the same for the α and β modifications of zirconium.

b - c : addition of oxygen to the oxygen-saturated metal to produce one mole of the oxide at the lower phase boundary (O/Zr = x). This reaction can be written as

$$Zr(\text{sat. with oxygen}) + \tfrac{1}{2}(2-y-x)O_2(g) = ZrO_{2-x} \qquad (4)$$

The heat released by this equilibrium reaction is:

$$Q_{b-c} = -\Delta H_R \qquad (5)$$

where $\Delta H_R$ is the standard enthalpy change of reaction (4).

c - d : dissolution of oxygen in the hypostoichiometric oxide to produce perfect stoichiometry corresponds to the reaction:

$$O_2(g) = 2O(\text{sol'n in oxide}) \qquad (6)$$

and the heat release for this step is given by:

$$Q_{c-d} = -\tfrac{1}{2}\int_0^x \overline{\Delta H}_{ox} dx' \qquad (7)$$

where $\overline{\Delta H}_{ox}$ is the partial molar enthalpy of oxygen in $ZrO_{2-x}$, which is a function of the O/Zr ratio.

The sum of the heat releases in the three steps is equal to the negative of the heat of combustion of pure zirconium:

$$\Delta H^o_f ZrO_2 = \tfrac{1}{2}\ \overline{\Delta H}_M y + \Delta H_R + \tfrac{1}{2}\int_0^x \overline{\Delta H}_{ox} dx' \qquad (8)$$

The components of Eq(8) are evaluated below for an isotherm at 1300°C.

The heat formation of zirconium dioxide at 298 K is given in ref. 1 as -263 kcal/mole. Extrapolating to 1300°C taking into account the difference in heat capacities of products and reactants (also given in Ref. 1) gives

$\Delta H^{o}_{f}ZrO_2$ = - 260 kcal/mole.

Komarek and Silver (2) measured the oxygen pressures in equilibrium with solutions of oxygen in α-Zr. Their data yield a heat of solution $\overline{\Delta H_M}$ = - 272 kcal at 10-15 at % oxygen and a variation of ∿13 kcal/mole between infinite dilution and saturation. From Fig. 1, the saturated α phase contains ∿30 atom percent oxygen (O/Zr = 0.43) at 1300°C, so that the first term on the right hand side of Eq (8) is ½ $\overline{\Delta H_M}y \simeq -58$ kcal/mole.

The only work that provides some information on the partial molar enthalpy of solution of oxygen in $ZrO_2$ is that of Aronson(3). Unfortunately, the oxygen potential he obtained changes temperature dependence across the $ZrO_{2-x}$ phase field in a manner which implies changes in the signs of $\overline{\Delta H_{ox}}$ and the partial molar entropy of solution, $\overline{\Delta S_{ox}}$. This unusual behavior may be due to the fact that the temperature range of the experiments (900 - 1100°C) spanned the monoclinic-tetragonal transition temperature of zirconia (1000°C). Rather than accept the odd variation of $\overline{\Delta H_{ox}}$ with O/Zr implied by these data, we use only the oxygen potentials at 1100°C, which apply to tetragonal zirconia. These data, in conjunction with a theoretical estimate of $\overline{\Delta S_{ox}}$, determines $\overline{\Delta H_{ox}}$ by:

$$\overline{\Delta H_{ox}} = \overline{\Delta G_{ox}} + T\,\overline{\Delta S_{ox}} \qquad (9)$$

The tetragonal structure of zirconia is simply a distorted fluorite lattice (4) and the dominant point defects in the nonstoichiometric compound are oxygen vacancies. Consequently, $\overline{\Delta S_{ox}}$ of $ZrO_{2-x}$ should behave in a manner similar to other oxygen-deficient oxides with the fluorite structure, such as $(U,M)O_{2-x}$ where M is another cation. Wadier (5) has shown that $\overline{\Delta S_{ox}}$ for the hypostoichiometric mixed uranium-neodymium oxide can be satisfactorily represented by a simple model which assumes a perfect cation sublattice and isolated vacancies on the anion sublattice. The partial molar entropy of solution is given by:

$$\overline{\Delta S_{ox}} = 2\overline{S}_O - S^{o}_{O_2} \qquad (10)$$

where $S^o_{O_2}$ is the entropy of molecular oxygen and $\bar{S}_O$ is the partial molar entropy of oxygen ions in $ZrO_{2-x}$. The former consists primarily of a translational entropy contribution with a smaller contribution from rotation. At 1300°C, the methods described in Ref. 6 give the value $S^o_{O_2} \simeq 50$ eu.

Following Wadier(5), we assume that $\bar{S}_O$ is purely configurational. The entropy of mixing $N_O$ oxygen ions on $N_s$ oxygen ion sites is:

$$S_{mix} = -R\left\{N_O \ln(N_O/N_s) + (N_s - N_O)\ln([N_s - N_O])/N_s\right\} \qquad (11)$$

where R is the gas constant, $\bar{S}_O$ is given by: (12)

$$\bar{S}_O = \left(\frac{\partial S_{mix}}{\partial N_O}\right)_{N_s}$$

performing the differentiation and noting that $N_O/N_s = 1 - \frac{1}{2}x$ results in:

$$\bar{S}_O = -R\ln\left(\frac{2-x}{x}\right) \qquad (13)$$

which is Wadier's result(5).

Using this estimate of $\overline{\Delta S}_{ox}$ and Aronson's values of $\overline{\Delta G}_{ox}$ at 1100°C in Eq(9) yields the partial molar enthalpy of solution shown in Fig.2. Although there is no way of accurately estimating $\overline{\Delta H}_{ox}$ at exact stoichiometry (because of the mathematical form of Eq(13)), the shape and magnitude of the curve in Fig. 1 are consistent with those observed for $(U,Pu)O_{2-x}$(7). With the lower phase boundary at 1300°C equivalent to the composition $ZrO_{1.84}$, the last term in Eq(8) is approximately -20 kcal/mole. Using these estimates of the heats of solutions in the metal and in the oxide in Eq(8), the enthalpy of reaction (4) at 1300°C is calculated to be $\Delta H_R \simeq -182$ kcal/mole. Analogous estimates at other temperatures can be obtained by using the phase diagram values of the compositions x and y. The solubility of oxygen in α - Zr is nearly temperature independent but the lower phase boundary of $ZrO_{2-x}$ is given by Pawel(8) as $x \simeq 10^{-4}T(K)$.

## III HEAT RELEASE DURING ZIRCALOY OXIDATION

Corrosion kinetics are customarily expressed as the rate of weight gain and the rate of growth of the oxide scale. In the case of zirconium oxidation, a layer of oxygen-stablized α - Zr forms between the oxide scale and the substrate. In the present analysis, the α - Zr layer is not distinguished from the remaining β-Zr because the two phases are assumed to have

similar thermal properties. Figure 3 shows typical scale formation on Zircaloy. The points labeled a,b, c and d correspond to those in Fig. 1 Because the change in O/Zr ratio across the oxide phase is small, the segment d - c of the oxygen distribution is assumed to be a straight line.

If the initial thickness of the oxygen-free zirconium slab is $L_{Mo}$ and $L_M$ and $L_{ox}$ denote the thickness of metal ($\alpha + \beta$) and oxide at time t, conservation of zirconium leads to:

$$\rho_M(L_{Mo} - L_M) = \rho_{ox}L_{ox} \tag{14}$$

$\rho_M$ and $\rho_{ox}$ are numbers of gram atoms of zirconium per unit volume of metal and oxide, respectively. The ratio $\rho_M/\rho_{ox}$ is approximately 1.5.

In a time interval $\Delta t$ the results of oxidation is:

$\Delta N_T$ = uptake of oxygen (g atoms/cm$^2$) in $\Delta t$

$\Delta L_{ox}$= increase in oxide layer thickness in $\Delta t$

The number of gram atoms of zirconium contained in a unit area of oxide scale is $\rho_{ox}L_{ox}$, and the average O/Zr ratio of the scale is at all times equal to $2 - \frac{1}{2}x$. Therefore, the change in the amount of oxygen bound in the oxide scale as a result of the increase of $\Delta L_{ox}$ in thickness is $(2 - \frac{1}{2}x)\,\rho_{ox}L_{ox}$ However, the oxide scale grows by converting $\rho_{ox}\Delta L_{ox}$ g atoms per cm$^2$ of adjacent zirconium metal which is saturated with oxygen. Thus, of the change in the amount of oxygen in the scale, an amount $y\rho_{ox}\Delta L_{ox}$ is supplied by the converted metal, with the remainder,

$$\Delta N_{ox} = (2-\tfrac{1}{2}x-y)\,\rho_{ox}\Delta L_{ox} \tag{15}$$

being supplied from the total uptake from the oxidizing gas. The difference,

$$\Delta N_M = \Delta N_T - \Delta N_{ox} \tag{16}$$

is the quantity of oxygen which enters the metal phase during the time interval $\Delta t$.

In determining the heat release, the partial molar heats of solution of oxygen in the metal and in the oxide are considered to be independent of composition. The consequence of this assumed behavior is the absence of heat release in the bulk oxide and metal phases due to oxygen diffusion

down concentration gradients. The heat effects of corrosion are localized at the interfaces between the gas and the oxide and between the oxide and the metal.

For oxidation in steam, the heat released at the gas-oxide interface consists of two components. The total quantity of oxygen entering the specimen in time $\Delta t$ must first be produced by decomposing water:

$$H_2O(g) = H_2(g) + \tfrac{1}{2}O_2(g) \qquad (17)$$

for which the heat release is the standard heat of formation of water. At 1300°C $\Delta H^{o}_{fH_2O}$ = - 59 kcal/mole. The oxygen gas is dissolved in the surface of the oxide according to Equation (6) for which the heat released per mole of oxygen is $-\frac{1}{2}\,\overline{\Delta H}_{ox}$. Thus, the heat release at the gas-oxide surface is:

$$\Delta Q_{g-ox} = \left(-\tfrac{1}{2}\,\overline{\Delta H}_{ox} + \Delta H^{o}_{fH_2O}\right)\Delta N_T \qquad (18)$$

Taking an average value of the partial molar enthalpy of solution of oxygen in the oxide to be -250 kcal/mole (Fig.2), the heat release at the gas-oxide surface is:

$$\Delta Q_{g-ox} = 2.8\times10^{5}\,\Delta N_T \qquad (J/cm^2) \qquad (19)$$

Despite the endothermicity of Reaction (17), the large energy release upon incorporation of gaseous oxygen in the oxide makes the overall surface reaction exothermic.

The $\Delta N_T$ g atoms of oxygen entering the surface ultimately appear in one of three locations. An amount $\Delta N_M$ enters the metal at the oxide-metal interface where the heat released is $(\frac{1}{2}\,\overline{\Delta H}_{ox} - \frac{1}{2}\overline{\Delta H_M})\Delta N_M$. An amount $(2-x-y)\rho_{ox}\ \Delta L_{ox}$ reacts with the metal at the oxide-metal interface to produce $ZrO_{2-x}$. The heat released at this interface by this process is $(2-x-y)\rho_{ox}\ \Delta L_{ox}(\frac{1}{2}\,\overline{\Delta H}_{ox}) - \Delta H_R \rho_{ox}\Delta L_{ox}$. The remaining $\frac{1}{2}x\,\rho_{ox}\Delta L_{ox}$ g atoms of oxygen stay in the oxide and so contribute nothing more to the heat release. Adding these contributions and eliminating $\Delta N_M$ by using Eqs(15)

and (16) yields:

$$\Delta Q_{ox-M} = \tfrac{1}{2}(\overline{\Delta H}_{ox} - \overline{\Delta H}_{M})\Delta N_T - \left[\Delta H_R + \tfrac{1}{4}x\overline{\Delta H}_{ox} - (2-y-\tfrac{1}{2}x)(\tfrac{1}{2}\overline{\Delta H}_{M})\right]\rho_{ox}\Delta L_{ox} \tag{20}$$

Inserting numerical values for the thermodynamic properties in Eq(20) yields:

$$\Delta Q_{ox-M} = 4.6\times10^4\,\Delta N_T - 4.5\times10^4\,\rho_{ox}\Delta L_{ox} \tag{21}$$

These heat release values are quite sensitive to the variation of $\overline{\Delta H}_{ox}$ with composition of the oxide. The function shown in Fig. 2 can be represented by:

$$\overline{\Delta H}_{ox} = (\overline{\Delta H}_{ox})_0 - ax' + bx'^2 \tag{22}$$

which shows that the partial molar enthalpy of oxygen in the oxide at the gas-oxide interface is $(\overline{\Delta H}_{ox})_0$ = -162 kcal/mole. For the curve in Fig. 2, a = 2000 kcal/mole and b = 8400 kcal/mole. If the heat release analysis is performed with $\overline{\Delta H}_{ox}$ given by Eq(22) instead of by a constant, the heat source at the interfaces are still given by Eqs(18) and (20) but the partial molar enthalpy in the oxide appearing in these formulas is replaced by its value for stoichiometric zirconia, which is $(\overline{\Delta H}_{ox})_0$. The heat releases at the interfaces at 1300°C become:

$$\Delta Q_{g-ox} = 9.2\times10^4\,\Delta N_T \qquad (J/cm^2) \tag{23}$$

$$\Delta Q_{ox-M} = 2.3\times10^5\,\Delta N_T - 6.1\times10^4\,\rho_{ox}\Delta L_{ox} \qquad (J/cm^2) \tag{24}$$

In addition there is a bulk heat release in the oxide scale which is given by:

$$\Delta Q_{ox} = \tfrac{1}{2}x\,\rho_{ox}\Delta L_{ox}\left(\tfrac{1}{3}ax - \tfrac{1}{4}bx^2\right) = 1.8\times10^4\,\rho_{ox}\Delta L_{ox} \quad (J/cm^2) \tag{25}$$

The principal effect of the concentration dependence of $\overline{\Delta H}_{ox}$ is a reduction by a factor of three in the heat source at the gas-oxide interface and an increase in the heat released at the oxide-metal interface. The bulk heating of the oxide layer is relatively minor.

## IV EFFECT OF THE HEAT OF REACTION ON THE TEMPERATURE DISTRIBUTION

All experimental studies of Zircaloy corrosion by steam assume a uniform temperature distribution within the reacting sample. However, temperature nonuniformities may result from the partitioning of the heat release between the gas-oxide and oxide-metal interfaces. Similarly, the location of the heat release due to oxidation may have a significant effect on calculation of cladding temperatures in a reactor accident situation which involves oxidation of Zircaloy.

To assess the importance of the heat source location on the temperature distribution, the following idealized situation is analyzed. We assume that a slab specimen of metal is placed in a furnace. Heat transfer between the furnace, and the specimen is assumed to occur solely by radiation; for simplicity convective heat transfer to the gas phase is neglected. In the absence of chemical reaction, the specimen acquires the temperature of the furnace, which is maintained constant at $T_o = 1300^oC$ at all times. Steam is admitted at time zero and oxidizes the slab from both sides. Thus, the midplane of the specimen is adiabatic for heat transfer purposes. The half-thickness of the specimen, $L_{Mo}$, is assumed sufficiently large so that the oxygen diffusion process occurs as in an infinite medium. Finally, we assume that oxidation kinetics are those at the base temperature $T_o$; acceleration of the corrosion rate by the heat released is neglected. Our object is to obtain a first estimate of the temperature nonuniformities caused by discrete heat sources in the slab. A realistic calculation would have to couple the corrosion kinetics with the thermal analysis. The heating of the interfaces is coupled to the corrosion rate via Eqs(19) and (21), which apply to the case of constant heat of solution of oxygen in the oxide. Bulk heating of the oxide scale is not considered.

The heat source at the gas-oxide interface is:

$$q_{g-ox} = \frac{\Delta Q_{g-ox}}{\Delta t} = 2.8\times10^5 \frac{\Delta N_T}{\Delta t} = \frac{2.8\times10^5\, k_T}{\sqrt{t}} = \frac{\phi}{\sqrt{t}} \tag{26}$$

where $k_T$ is the parabolic rate constant for the weight gain and $\phi = 2.8 \times 10^5\, k_T$. Similarly, the heat source at the oxide-metal is:

$$q_{ox-M} = \frac{\Delta Q_{ox-M}}{\Delta t} = 4.6\times10^4 \frac{\Delta N_T}{\Delta t} - 4.5\times10^4\, \rho_{ox} \frac{\Delta L_{ox}}{\Delta t} \tag{27}$$

The zirconium density in the oxide is $\rho_{ox} = 0.0472$ g at Zr/cm$^3$. The velocity of the oxide-metal boundary is equal to $\Delta L_{ox}/\Delta t$, for which the parabolic rate constant $k_{ox}$ is also available from Ref. 9:

$$v = \frac{\Delta L_{ox}}{\Delta t} = \frac{k_{ox}}{\sqrt{t}} \qquad (cm/s) \tag{28}$$

Combining the above information, the oxide-metal interfacial heat source is:

$$q_{ox-M} = \Omega/\sqrt{t} \tag{29}$$

The units of $\phi$ of Eq (26) and $\Omega$ in Eq(29) are J/cm$^2$-s$^{\frac{1}{2}}$. The strength of the heat source at the gas-oxide boundary is $\sim$ 9 times that at the oxide-metal interface. However, as discussed in the preceding section, this split is very sensitive to the magnitude and the concentration-dependence of the partial molar heat of solution of oxygen in the oxide.

The heat balance at the gas-oxide interface (z=0) is:

$$h\left[T_{ox}(0) - T_\infty\right] = \kappa_{ox}\left(\frac{\partial T_{ox}}{\partial z}\right)_0 + q_{g-ox} \tag{30}$$

where $\kappa_{ox}$ is the thermal conductivity of the oxide and $T_{ox}$ is its

temperature. The left hand side of Eq(30) represents the heat flux from the surface to the surroundings, for which h is the appropriate heat transfer coefficient.

Because of the oxide scale is thin, the temperature distribution in this region can be assumed to be in quasi-steady state.

This assumption can be justified by nondimensionalizing the heat conduction equation in the oxide scale and examing the magnitude of the terms in the resulting equation. The scale factor for the distance is the initial specimen half-thickness:

$$\eta = z/L_{MO} \tag{31}$$

A characteristic time is defined in terms of the growth kinetics of the oxide scale. The fraction of the initial metal converted to oxide is obtained from Eq(14):

$$\frac{L_{MO} - L_M}{L_{MO}} = \frac{\rho_{ox}}{\rho_M} \frac{L_{ox}}{L_{MO}} \tag{32}$$

The thickness of the oxide scale is given by the integral of Eq(28) and a dimensionless time is defined by:

$$\tau = \frac{L_{MO} - L_M}{L_{MO}} = C_2\sqrt{t} \tag{33}$$

where:

$$C_2 = \frac{2}{1.5} \frac{k_{ox}}{L_{MO}} \quad (s^{-\frac{1}{2}}) \tag{34}$$

The Pilling-Bedworth ratio ($\rho_M/\rho_{ox}$) is 1.5 for $Zr/ZrO_2$.

In terms of the dimensionless quantities defined by Eq(31) and (33), the heat conduction equation in the oxide is:

$$\frac{\partial^2 \theta_{ox}}{\partial \eta^2} = \frac{1}{2\tau}\left[\frac{L_{MO}^2/\alpha_{ox}}{1/C_2^2}\right]\frac{\partial \theta_{ox}}{\partial \tau} \qquad (35)$$

where $\alpha_{ox}$ is the thermal diffusivity of $ZrO_2$ and $\Theta_{ox}$ is the dimensionless temperature:

$$\Theta_{ox} = \frac{T_{ox} - T_o}{T_o} \qquad (36)$$

The numerator of the bracketed term in Eq(35) is the characteristic thermal response time of the oxide and the denominator is the characteristic scale growth time. Taking $L_{MO}$ = 0.05 cm and $\alpha_{ox}$ = $7X10^{-3}$ $cm^2/s$, the bracketed term in Eq(35) is $2x10^{-5}$. Thus, except for times very close to zero, the temperature distribution in the oxide scale is to good approximation a linear function of distance:

$$\frac{T_{ox} - T_o}{T_o} = A + B\left(\frac{z}{L_{MO}}\right) \qquad (37)$$

Because the thermal conductivity of the metal is very large, the thermal response of the metal phase can be treated as a lumped capacity and temperature gradients neglected. The oxide-metal interface moves with velocity v towards the midplane of the slab, which is equivalent to an adiabatic boundary. The energy balance over a volume contained between a plane on the oxide side of the oxide-metal interface and the slab midplane is:

$$\rho_M C_{pM} \frac{d}{dt}\left[L_M(T_M - T_o)\right] = -\rho_{ox} C_{pox}\, v(T_M - T_o) + q_{ox-M} - \chi_{ox}\left(\frac{dT_{ox}}{dz}\right) \qquad (38)$$

where $\rho_{ox}C_{pox}$ and $\rho_M C_{pM}$ are the heat capacities per unit volume of the oxide and metal, respectively, and $T_M$ is the metal temperature.

The first term on the right hand side of this equation represents the sensible heat carried by the oxide moving away from the interface in the moving coordinate system. The metal layer thickness on the left hand side of the equation is obtained from Eq(33) and a dimensionless metal temperature is defined by:

$$\theta = \frac{T_M - T_o}{T_o} \tag{39}$$

The derivative on the right hand side of Eq(38) is evaluated from Eq(37), the velocity v is given by Eq(27) and $q_{ox-M}$ is taken from Eq(38). These substitutions and use of Eq(39) transform Eq(38) into

$$-C_1 \frac{d}{dt}\left[\theta(1-C_2\sqrt{t})\right] - C_3 \frac{\theta}{\sqrt{t}} + \frac{\Omega}{\sqrt{t}} = C_4 B \tag{40}$$

where: (41)

$$C_1 = \rho_M C_{pM} L_{Mo} T_o \qquad (J/cm^2)$$

$$C_3 = k_{ox}\, \rho_{ox} C_{pox} T_o \qquad (J/cm^2\text{-}s^{\frac{1}{2}}) \tag{42}$$

$$C_4 = \kappa_{ox} T_o / L_{Mo} \qquad (W/cm^2) \tag{43}$$

Using Eqs(37) and (39), the temperature match at the oxide-metal interface becomes:

$$\theta = A + B(L_{ox}/L_{Mo})$$

or, using Eqs(32) and (33) to determining $L_{ox}/L_{Mo}$, this equation is:

$$\theta = A + 1.5 C_2 B \sqrt{t} \tag{44}$$

The heat balance at the gas-oxide interface, Eq(29), can also be expressed in dimensionless terms. Eliminating $T_{ox}$ in this equation by use of Eq(37) and inserting the heat source strength give by Eq(26) gives:

$$C_5 A = C_4 B + \phi / \sqrt{t} \tag{45}$$

where $C_5 = hT_o \quad (W/cm^2)$ (46)

Eliminating A between Eqs(44) and (47) and solving the resulting equation for B yields:

$$B = \frac{C_5\theta - \phi/\sqrt{t}}{C_4 + 1.5C_2C_5\sqrt{t}} \tag{47}$$

Substituting Eq(47) into Eq(40) gives

$$-C_1\frac{d}{dt}\left[\theta(1-C_2\sqrt{t})\right] - C_3\frac{\theta}{\sqrt{t}} + \frac{\Omega}{\sqrt{t}} = \frac{C_5\theta - \phi/\sqrt{t}}{1 + \frac{1.5C_2C_5}{C_4}\sqrt{t}} \tag{48}$$

Using the dimensionless time defined by Eq(33) converts Eq(48) to:

$$\tfrac{1}{2}(1-\tau)\frac{d\theta}{d\tau} - \left(\frac{1}{2} - \frac{C_3}{C_1C_2}\right)\theta - \frac{\Omega}{C_1C_2} = -\frac{\frac{C_5}{C_1C_2^2}\tau\theta - \frac{\phi}{C_1C_2}}{1 + \frac{1.5C_5}{C_4}\tau} \tag{49}$$

which is to be solved with the initial condition $\theta = 0$ at $\tau = 0$.

Table 1 shows the parameters used in solving Eq(49). The two methods of estimating the internal heat source described in Section III were tested. These correspond to the case of constant partial molar enthalpy of solution of oxygen in the oxide and to the case of the concentration-dependent $\overline{\Delta H_{ox}}$. As shown in Table 1, these two estimates lead to very different partitioning of the heat source between the gas-oxide and the oxide-metal interfaces, even though the total heat release ($\phi + \Omega$) is the same in both instances. In addition, the heat transfer coefficient between the oxide surface and the specimen surroundings was varied from the adiabatic limit h = 0 to the limit of very rapid cooling ($h = \infty$). An intermediate case corresponding to heat removal by radiation alone, for which $h = 4\ \sigma\varepsilon T_o^3$ was tested. Here $\sigma$ is the Stefan-Boltzmann constant and $\varepsilon$ is the system emissivity. For $\varepsilon = 0.7$ and $T_o = 1300^oC$, $C_5 = hT_o = 100 W/cm^2$.

In all cases, the calculations showed that despite the low thermal conductivity of $ZrO_2$, temperature gradients across the oxide scale were negligible. Except for very large surface heat transfer coefficients, the denominator of the right hand side of Eq(49) is very close to unity. A consequence of this behavior is that the thermal behavior of the system is independent of the manner in which the heat of oxidation is partitioned between the gas-oxide and the oxide-metal interfaces and depends only on the total heat release parameter $\phi + \Omega$. When h is very large, the calculated temperature rise of the specimen is approximately zero in both the oxide and metal phases.

The results of these calculations demonstrate that the thermal response of the thin metal specimens to oxidation can be represented by the gradient-free lumped capacity heat balance:

$$C_1 \frac{d\theta}{dt} = q(t) - C_5\theta \qquad (50)$$

where $\theta$ now refers to the specimen temperature without distinction between oxide and metal and q(t) is the total heat release rate at both interfaces. In the calculations described above, $q(t) = (\phi + \Omega)/\sqrt{t}$.

## V APPROXIMATE COUPLING OF CORROSION KINETICS AND THERMAL RESPONSE

The analysis presented in Section IV was based upon the assumption

Table 1 Parameters for the Thermal Analysis

Ambient temperature $T_o = 1300^{\circ}C$

Specimen half-thickness $L_{Mo} = 0.05$ cm

Parabolic rate constants at $1300^{\circ}C$ ( Ref. 9)

weight gain $k_T = 3.1 \times 10^{-5}$ g atoms oxygen/$cm^2$- $s^{\frac{1}{2}}$

oxide scale $k_{ox} = 2.4 \times 10^{-4}$ cm/$s^{\frac{1}{2}}$

Internal heat sources due to oxidation ($J/cm^2$ - $s^{\frac{1}{2}}$) (see Sec. IV):

constant $\overline{\Delta H_{ox}}$: $\phi = 8.68$; $\Omega = 0.92$

variable $\overline{\Delta H_{ox}}$: $\phi = 2.85$; $\Omega = 6.64$

Heat Capacities (Ref. 10):

$C_{pox} = 0.60$ J/g-K

$C_{pM} = 0.38$ J/g-K

Densities: (Ref (10):

$\rho_{ox} = 0.0472$ g atoms Zr/$cm^3$ (5.82 g/$cm^3$)

$\rho_M = 0.0712$ g atoms Zr/$cm^3$ (6.49 g/$cm^3$)

Oxide thermal conductivity (10): $\kappa_{ox} = 0.024$ W/cm -K

Combined Parameters:

$C_1 = 194$ J/$cm^2$

$C_2 = 6.4 \times 10^{-3}$ $s^{-\frac{1}{2}}$

$C_3 = 1.32$ J/$cm^2$ -$s^{\frac{1}{2}}$

$C_4 = 755$ W/$cm^2$

$C_5$ = varied

that the temperature rise due to release of the heat of oxidation did not affect the corrosion kinetics. This assumption can be removed and coupling of the heat and mass transport processes achieved by the following approximate method. An approximation adopted by Markworth (11) consists of assuming that the basic parabolic scaling laws apply in the temperature transient but the scaling coefficients are thermally activated. With this simplication, the rate of weight gain is given by:

$$\frac{dN_T}{dt} = \frac{k_T}{\sqrt{t}} \exp\left[ - \frac{E_T}{R}\left(\frac{1}{T} - \frac{1}{T_o}\right)\right] \tag{51}$$

where $k_T$ is the parabolic rate constant at temperature $T_o$, $E_T$ is the activation energy for the weight gain parameter determined by isothermal corrosion experiments at various temperatures, and R is the gas constant.

Similarly, Eq(28) is generalized to:

$$v = \frac{dL_{ox}}{dt} = \frac{k_{ox}}{\sqrt{t}} \exp\left[ - \frac{E_{ox}}{R}\left(\frac{1}{T} - \frac{1}{T_o}\right)\right] \tag{52}$$

where $k_{ox}$ is the parabolic rate constant for oxide scale growth at temperature $T_o$ and $E_{ox}$ is its activation energy.

The activation energies are given in Ref. 9 as $E_T$ = 20 kcal/mole and $E_{ox}$ = 18 kcal/mole. Substituting Eqs(51) and (52) into Eqs(26) and (27) and summing the two, the oxidation heat source in the thermal analysis becomes:

$$q = 3.26 \times 10^5 \, k_T \, e^{6.4\Theta} - 2.12 \times 10^3 \, k_{ox} \, e^{5.7\Theta} \tag{53}$$

where $\Theta$ is the dimensionless temperature defined by Eq(39). It is dependent on time but not on position and is determined by solution of Eq(50) with the heat source give by Eq(53).

## VI ACCURATE COUPLING OF HEAT AND MASS TRANSPORT DURING CORROSION

The major shortcoming implicit in the coupling method described in the

previous section is the description of the corrosion process by parabolic kinetics in a temperature transient. This is in principle wrong, because parabolic kinetics requires time-independent parameters such as oxygen diffusion coefficients and interface concentrations. Thus application of Eqs(51) and (52) to situations with time-dependent temperatures is open to question. This deficiency can be eliminated by analyzing the corrosion process from the same basic principles that have been applied to isothermal corrosion kinetics. The material properties are permitted to be time-dependent but the temperature is assumed to be spatially independent because the demonstration of this property in Section IV remains valid.

The kinetics of oxidation are determined by solving the oxygen diffusion equations in the oxide and metal zones of the specimen and matching fluxes and concentrations at the metal-oxide interface. This technique has been used by Pawel (12) to analyze isothermal oxidation of Zircaloy. We apply the same type of analysis to the present transient problem with the aid of the following simplifications:

I) The oxygen concentration profile in the oxide layer is assumed to be a linear function of distance.

II) The distinction between α-Zr and β-Zr is neglected.

III) The system is semi-infinite insofar as oxygen penetration is concerned.

The system is depicted in Fig. 3. Because of the volume change upon oxidation, the metal lattice moves away from the gas-oxide interface with a velocity denoted by $v_{Zr}$. This motion can be related to the velocity of the oxide-metal interface by using the zirconium balance given by Eq(14). From Fig. 3

$$v_{Zr} = \frac{d}{dt}(L_{ox} + L_M)$$

and from Eq(14):

$$\frac{dL_M}{dt} = -\frac{\rho_{ox}}{\rho_M}\frac{dL_{ox}}{dt} = -\frac{1}{1.5}\frac{dL_{ox}}{dt}$$

Combining these two equations and noting that $dL_{ox}/dt = v$ yields:

$$v_{Zr} = v/3 \tag{54}$$

Because the oxygen distribution in the oxide layer has been assumed to be linear, we may write:

$$\frac{C_d - C_{ox}}{C_d - C_c} = \frac{z}{L_{ox}} \tag{55}$$

where $C_{ox}$ is the oxygen concentration at location z in the oxide layer and $C_d$ and $C_c$ are the boundary concentrations of oxygen at points d and c in Fig. 3, respectively. These correspond to stoichiometric zirconia and to substoichiometric zirconia at the lower phase boundary.

In the metal phase the oxygen conservation equation is:

$$\frac{\partial C_M}{\partial t} = \frac{\partial J}{\partial z'} \tag{56}$$

where $C_M$ is the oxygen concentration in the metal and J is the oxygen flux in the metal phase with respect to the coordination origin of $z'$, which is chosen as the moving oxide-metal interface. This flux consists of two terms, a Fick's law component representing oxygen diffusion relative to the zirconium lattice and a convective term reflecting movement of the zirconium lattice with respect to the oxide metal interface. The convective velocity is the difference between the lattice velocity with respect to the fixed gas-oxide interface and the velocity of the oxide-metal interface with respect to the same plane:

$$v_M = v_{Zr} - v = - v/1.5 \tag{57}$$

The oxygen flux in the metal is:

$$J = - D_M \frac{\partial C_M}{\partial z'} + v_M C_M \tag{58}$$

where $D_M$ is the diffusion coefficient of oxygen in the metal. Combining Eqs(56) - (58) gives the oxygen diffusion equation in the metal phase:

$$\frac{\partial C_M}{\partial t} - \frac{v}{1.5} \frac{\partial C_M}{\partial z'} = D_M \frac{\partial^2 C_M}{\partial z'^2} \tag{59}$$

The initial and boundary conditions are:

$$C_M(z',0) = 0 \tag{60}$$

$$C_M(0,t) = C_b \tag{61}$$

$$C_M(\infty,t) = 0$$

where $C_b$ is the saturation concentration of oxygen in α - Zr. The last condition embodies the semi-infinite medium condition and neglects the transformation from α - Zr to β - Zr.

Equality of oxygen fluxes in the oxide and metal phases at the interface is expressed by:

$$-D_{ox}\left(\frac{\partial C_{ox}}{\partial z}\right)_{L_{ox}} - vC_c = -D_M\left(\frac{\partial C_M}{\partial z'}\right)_0 - \frac{v}{1.5}C_b \tag{62}$$

where $D_{ox}$ is the oxygen diffusivity in $ZrO_2$.

If the diffusion coefficient and the boundary concentrations are all constant, the velocity in Eqs(59) and (62) is $v = k_{ox}/\sqrt{t}$, where $k_{ox}$ is the parabolic scaling constant, and the solution to Eq(59) is:

$$\frac{C_M}{C_b} = \frac{\operatorname{erfc}\left(\frac{z'}{2\sqrt{D_M t}} + \frac{k_{ox}}{1.5\sqrt{D_M}}\right)}{\operatorname{erfc}\left(\frac{k_{ox}}{1.5\sqrt{D_M}}\right)} \tag{63}$$

Substituting Eqs(55) and (63) into Eq(62) and noting that $L_{ox} = 2k_{ox}\sqrt{t}$ yields:

$$\frac{D_{ox}(C_d - C_c)}{2k_{ox}} - k_{ox}(C_c - C_b/1.5) = C_b\left(\frac{D_M}{\pi}\right)^{\frac{1}{2}} \frac{\exp\left[-\left(\frac{k_{ox}}{1.5\sqrt{D_M}}\right)^2\right]}{\operatorname{erfc}\left(\frac{k_{ox}}{1.5\sqrt{D_M}}\right)} \tag{64}$$

The kinetic equation for the rate of weight gain is obtained from:

$$\frac{dN_T}{dt} = -D_{ox}\left(\frac{\partial C_{ox}}{\partial z'}\right)_0 = \frac{k_T}{\sqrt{t}}$$

or:

$$k_T = \frac{D_{ox}(C_d - C_c)}{2k_{ox}} \tag{65}$$

The isothermal rate constant $k_{ox}$ and $k_T$ can be determined by using the oxygen diffusion coefficients and interface concentrations in Eqs (64 and (65). Using the following data given in Ref. 12 for 1300°C:

$$C_d = 2\rho_{ox} = 0.094 \text{ g atoms oxygen /cm}^3$$
$$C_c/C_d = 1.84/2 = 0.092$$
$$C_b/C_d = 0.31$$
$$D_{ox} = 2.0 \times 10^{-6} \text{ cm}^2 \text{ /s}$$
$$D_M = 3.2 \times 10^{-7} \text{ cm}^2 \text{ /s (for } \alpha\text{-Zr)}$$

Eq (64) gives $k_{ox} = 2.5 \times 10^{-4}$ cm/s$^{\frac{1}{2}}$ and Eq (65) yields $k_T = 3.5 \times 10^{-5}$ g atoms oxygen /cm$^2$-s$^{\frac{1}{2}}$. These results are in excellent agreement with the data (see Table 1, ) which is not surprising since these data were used by Pawel (12) to determine $D_{ox}$ and $D_M$. All that we have done is to reverse this process. However, the comparison does demonstrate the assumptions I and II given at the beginning of this section are adequate for the corrosion analysis, and will be retained in analyzing the transient case.

Analysis of diffusive transport when the diffusion coefficients are time-dependent is simplified by the spatial uniformity of the temperature. Because of this feature, the diffusion coefficients, which are functions of temperature, depend on time but not on position. As a consequence, the oxygen concentration distribution in the oxide and metal phases is still determined by Eqs (55) and (59), respectively and the oxygen flux match at the oxide-metal interface is correctly expressed by Eq (62). What is inapplicable in the case of time-dependent diffusion coefficients is the assumption of parabolic scaling expressed by the relationship $v = k_{ox}/\sqrt{t}$.

The diffusivity of oxygen in zirconium metal can be considered as a function of time via the temperature:

$$D_M = D_{Mo}\, f \tag{66}$$

where $D_{Mo}$ is the diffusion coefficent at temperature $T_o$ and the factor f is given by:

$$f = \exp\left[-\frac{E_{DM}}{R}\left(\frac{1}{T} - \frac{1}{T_o}\right)\right] = e^{16.3\theta} \tag{67}$$

where $E_{DM}$ = 51 kcal/mole is the activation energy of oxygen diffusion in α-Zr(12) and Θ is the dimensionless temperature defined by Eq(39).

The only other quantity with a significant temperature dependence is the product of the oxygen diffusivity in the oxide and the oxygen concentration driving force across the oxide layer. The former exhibits Arrhenius behavior, but the difference in O/Zr ratio between stoichiometric zirconia and the reduced oxide at the lower phase boundary is approximately proportional to the absolute temperature(12). However, the temperature-dependence of this product can be expressed in Arrhenius form with an activation energy slightly larger than that which characterize the diffusion coefficient in the oxide. Thus:

$$D_{ox}(C_d - C_c) = \left[D_{ox}(C_d - C_c)\right]_o g \qquad (68)$$

where the bracketed coefficient with the zero subscript is the diffusivity-driving force product at temperature $T_o$ and the factor g is:

$$g = \left(\frac{T}{T_o}\right)\exp\left[-\frac{E_{Dox}}{R}\left(\frac{1}{T} - \frac{1}{T_o}\right)\right] = e^{12.1\Theta} \qquad (69)$$

where $E_{Dox}$ = 34.5 kcal/mole is the activation energy of oxygen diffusion in the oxide phase (12).

Equation (66) is substituted into Eq(59) and a new time variable is defined by:

$$u = \int_0^t f dt' \qquad (70)$$

The result is:

$$\frac{\partial C_M}{\partial u} - \frac{v}{1.5f}\frac{\partial C_M}{\partial z'} = D_{Mo}\frac{\partial^2 C_M}{\partial z'^2} \qquad (71)$$

In analogous fashion, the derivative on the left hand side of Eq(62) is evaluated from Eq(55) and Eqs(66) and (68) used. This transforms the oxygen flux match to:

$$\frac{\left[D_{ox}(C_d - C_c)\right]_o g}{fL_{ox}} - \frac{v}{f}\left(C_c - \frac{C_b}{1.5}\right)_o = -D_{Mo}\left(\frac{\partial C_M}{\partial z'}\right)_o \qquad (72)$$

The temperature dependence of the difference $(C_c - C_b/1.5)$ is small and so this quantity is evaluated at $T_o$.

There is no exact analytical solution to Eqs (71) and (72) when f and g are arbitrary functions of the time variable u. However, an approximate analytical solution can be obtained by assuming that the ratio v/f is inversely proportional to $\sqrt{u}$:

$$\frac{v}{f} = \frac{k}{\sqrt{u}} \qquad (73)$$

where k is a constant which replaces the scaling constant $k_{ox}$ of the isothermal case.

The oxide scale thickness is the first term of Eq(72) is determined by:

$$L_{ox} = \int_0^t v\,dt' = k\int_0^t \frac{f(t')dt'}{\sqrt{u(t')}} = 2k\sqrt{u} \qquad (74)$$

where Eq(70) has been used.

Substituting Eq(73) into Eq(71) produces an equation whose form is identical to that for the isothermal situation. The solution for the transient temperature process is thus given by Eq(63) with $k_{ox}$ replaced by k, t by u, and $D_M$ by $D_{Mo}$. This solution is used to evaluate the derivative on the right hand side of Eq(72).

With $L_{ox}$ and v on the left hand side given by Eq(73) and (74), Eq(72) becomes:

$$\frac{\left[D_{ox}(C_d-C_c)\right]_o}{2k}\frac{g}{f} - k\left(C_c - \frac{C_b}{1.5}\right)_o = \left(\frac{D_{Mo}}{\pi}\right)^{\frac{1}{2}} C_b \frac{\exp\left[-\left(\frac{k}{1.5\sqrt{D_{Mo}}}\right)^2\right]}{\operatorname{erfc}\left(\frac{k}{1.5\sqrt{D_{Mo}}}\right)} \qquad (75)$$

Except for the ratio g/f in the first term on the left hand side, this equation is identical to its isothermal counterpart, Eq(64). Although the activation energies of the factors g and f are large, the ratio g/f is only slightly temperature dependent because the activation energies of $D_M$ and $D_{ox}$ are comparable and the fractional temperature rise in the transient is modest. Consequently the approximation g/f = 1 in Eq(75) is acceptable, from which there follows :

$$k = k_{ox}$$

The temperature function $\Theta(t)$ is determined by solution of Eq(50) wherein the heat source q is the sum of the gas-oxide and oxide-metal components given by Eqs(26) and (27), respectively. These in turn depend upon the corrosion kinetics through the quantities $dN_T/dt$ and $dL_{ox}/dt$. The rate of weight gain is equal to the flux of oxygen across the oxide layer:

$$\frac{dN_T}{dt} = \frac{D_{ox}(C_d-C_c)}{L_{ox}} = \frac{\left[D_{ox}(C_d-C_c)\right]_o}{2k_{ox}}\frac{g}{\sqrt{u}} = k_T\frac{g}{\sqrt{u}} \qquad (76)$$

Similarly, Eq(73) yields:

$$v = \frac{dL_{ox}}{dt} = \frac{k_{ox}f}{\sqrt{u}} \qquad (77)$$

Substituting Eqs(76) and (77) into Eqs(26) and (27) and using the values of $k_{ox}$ and $k_T$ given in Table 1 for 1300°C yields the heat source:

$$q = 10.1\frac{g}{\sqrt{u}} - 0.51\frac{f}{\sqrt{u}} \qquad (78)$$

The solution is accomplished by iteration. An initial guess of $\Theta(t)$ is obtained, either from the no-coupling solution described in Sect. IV or from the approximate coupling method of Sect. V. This guess determines the first estimate of the time-dependent functions f and g from Eqs(67) and (69). The new time variable u is computed from Eq(70) and Eq(78) then provides the oxidation heat source for the next iteration. The new temperature function is obtained by solving Eq(50), and the iteration process continues until the solution has converged. The growth of the oxide scale as a function of time is the calculated from Eq(74).

## VII RESULTS AND DISCUSSION

Figures 4 and 5 show the results of the thermal and corrosion kinetic analyses for a 1 mm thick slab of Zircaloy oxidized on both sides by steam at 1300°C.

Figure 4 shows the temperature transient calculated by the three methods described in previous sections: no-coupling of heat and chemical reaction (Sect. IV), approximate coupling by application of Arrhenius-type temperature dependences to the parabolic scaling constants (Sect. V), and the accurate coupling method wherein temperature influences the basic thermodynamic and transport properties of the reacting solid (Sect. VI). The results in Figs. 4 and 5 show that the approximate method of coupling produces poorer predictions than ignoring coupling entirely. The curves labled "accurate coupling" were obtained by iteration starting either from the no-coupling or approximate coupling inital guesses.

A substantial temperature perturbation occurs at the start of the oxidation process when the rates of oxygen uptake by the solid is highest, but the temperature eventually approaches the ambient value because the thick oxide scale considerably reduces the rate of corrosion and hence the strength of the heat source inside or on the surface of the specimen. Figure 5 shows that correct simultaneous solution of the heat and mass transport equations in the solid predicts a scale thickness which is $\sim$ 7 μm larger than that given by the theory of isothermal scaling. The approximate coupling analysis overestimates the extent of oxygen absorption.

The results are sensitive to the heat removal rates from the specimen. This factor is contained in the coefficient $C_5$, which was chosen as 100 W/cm$^2$ for preparing the curves of Figs. 4 and 5. When more effective heat transfer to the surroundings is simulated by increasing $C_5$ to 150 W/cm$^2$, the peak temperatures shown in Fig. 4 is reduced by 50°C and the oxide layer thicknesses are several percent less than those shown by the solid curve in Fig. 5.

Although radiating cooling provides a lower limit to the heat transfer coefficient in the case of a single tubular specimen in a laboratory test, comparable minimum heat removal capability is not assured in a bundle of tubes as in a nuclear reactor fuel assembly. Because each cladding tube is surrounded by other tubes which are undergoing comparable oxidation, radiant interchange between one tube and its environment is drastically reduced. Only convective heat transfer

to the flowing steam remains as a mechanism of removing the heat oxidation. In this case, the heat removal parameter $C_5$ could be considerably smaller than the value of 100 $W/cm^2$ used in the sample calculations presented here.

The temperature excursion shown in Fig. 4 is qualitatively very similar to that observed by Hagen[13] in a fuel rod simulation test. In this configuration, heat was supplied from a central tungsten rod inside an annular fuel stack clad in Zircaloy. A Zircaloy shroud was placed around the specimen to simulate the presence of surrounding fuel pins. Initially argon flowed in the annular gap between rod and shroud. Upon adding steam to the argon flow, the Zircaloy temperatures rose from the steady pretest value of 1700°C to 2200°C and returned to less than 1700°C in less than one minute. The time scale of the transient was thus very close to that shown in Fig. 4, in which the comparable duration is ∿1/2 minute. However, the amplitude of the experimental transient (500°C) was much larger than the one represented in Fig. 4(125°C). Moreover, in Hagen's experiment, the surface temperature following the transient was lower than it was prior to addition of steam.

The reason for the latter observation is the dominance of convection rather than radiation cooling in Hagen's test; radiative heat transfer was effectively reduced by the surrounding shroud, which reacted in much the same way as the cladding and thus did not provide a radiation heat sink. Addition of steam to the argon flow sufficiently increased the convective heat transfer coefficient to give temperatures lower than pre-reaction values when the Zircaloy had become oxidized to an extent that heat release by residual corrosion was small.

The larger amplitude of the temperature transient reported by Hagen compared to the one analyzed in this work is probably due to the higher initial temperature in the former. Since the scaling constants are thermally activated, the magnitude of the transient should be greater at higher temperatures. Moreover, the calculations were based on rate constants appropriate to a tetragonal zirconia scale while the experimental temperatures probably resulted in a cubic zirconia layer and, at least during part of the excursion, in liquid zirconium.

## VIII CONCLUSIONS

1. The energy released during oxidation of Zircaloy by steam appears as planar sources of heat at the gas-oxide and oxide-metal interfaces. To a good approximation, the sum of the heat releases at these two locations is equal to the rate of weight gain multiplied by the enthalpy change of the reaction of water vapor with zircaloy to produce hydrogen gas and zirconium dioxide. The portion released at the gas-oxide interface is equal to the partial molar enthalpy of oxygen solution in $ZrO_2$ less the heat of formation of water. Knowing the total heat release and the heat release at the surface, the heat source at the oxide-metal interface follows by difference. The principal difficulty in accurately assessing the partitioning of the heat release between the two interfaces is lack of reliable information on the partial molar enthalpy of solution of oxygen in $ZrO_2$.

2. The thermal response of the oxidizing metal to the heat released by the reaction is practically independent of the details of the location of the heat sources inside the specimen. Despite the low thermal conductivity of the $ZrO_2$ scale, spatial variations of temperature in the oxide and the metal phases are negligible. The temperature of the specimen as a function of time is determined by a lumped capacity heat balance which divides the reaction enthalpy into heat removal by external cooling or increase in specimen temperature.

3. The method of coupling the heat transfer problem with scale formation kinetics is critical to accurate modeling. The conventional technique of assuming Arrhenius temperature dependences of the parabolic scaling constants (which were determined by isothermal experiments at different temperatures) is in principle incorrect and in practice inaccurate. Linkage of heat and mass transfer must be performed by according the appropriate temperature dependences to the basic properties which enter the conservation laws, namely the equilibrium interface concentrations and the oxygen diffusion coefficients.

Acknowledgement

This work was supported by the Director, Office of Energy Research, Office of Basic Energy Sciences, Materials Sciences Division of the U.S. Department of Energy under Contract # DE-AC03-76SF0009

# REFERENCES


1. O. Kubaschewski and C.B. Alcock, "Metallurgical Thermochemistry", 5th Ed., Pergamon Press (1979)

2. K.L. Komarek and M. Silver, Proc. Symp. On Thermodynamics of Nuclear Materials, IAEA, Vienna, P 749 (1962)

3. S. Aronson, J. Electrochem. Soc. 108, 312 (1961)

4. R.C. Garvie, "Zirconium Dioxide and Some of its Binary Systems", in "High Temperature Oxides, Part II", A.M. Alper, Ed., Acdemic Press, (1970)

5. J.F. Wadier, "Phase Diagram and Thermodynamic Properties of the Uranium-Neodymium-Oxygen System", Tech. Rept. CEA-R-4507 (1973)

6. G.N. Lewis, M. Randall, K.S. Pitzer and L. Brewer, "Thermodynamics" 2nd Ed., McGraw-Hill (1961)

7. D.R. Olander, "Fundamental Aspects of Nuclear Reactor Fuel Elements", p. 153, Natl. Tech Info. Service (1976)

8. R.E. Pawel and J.J. Campbell, ASTM - STP 754, p 370 (1982)

9. R.E. Pawel, J.V. Cathcart and R.A. McKee, J. Electrochem. Soc., 126, 1105 (1979)

10. MATPRO - Version 11; a Handbook of Materials Properties for Use in the Analysis of Light Water Reactor Fuel Rod Behavior, NUREG/CR -0497, TREE-1280, Rev. 2, August 1981

11. A.J. Markworth, Met. Trans. A, 8A , 2014 (1977)

12. R.E. Pawel, J. Electrochem, Soc. 126, 1111 (1979)

13. S. Hagen, "Out-of-Pile Experiments on the High Temperature Behavior of Zry-4 Clad Fuel Rods", Sixth Inter, Conf. on Zirconium in the Nuclear Industry, Vancouver July (1982)

## Figure Captions

1. Zr-O equilibrium phase diagram; Urbanic, V.F., "Oxidation of Zirconium Alloys in Steam at 1000 to 1850°C," Zirconium in the Nuclear Industry ASTM STP 633, A. L. Lowe, Jr. and G.W. Parry, Eds., American Society for Testing and Materials, 1977, pp. 168-181.
2. Composition dependence of the partial molar enthalpy of solution of oxygen in zirconia.
3. Oxide scale growth and oxygen concentration distribution during steam oxidation of Zircaloy.
4. Temperature perturbation due to inability to rapidly remove reaction heat during oxidation of zircaloy at 1300°C. Heat removal parameter $C_5$ = 100 W/cm$^2$. Three methods of calculating the temperature transient are represented.
5. Oxide scale growth during reaction in the temperature transient displayed in Fig. 4. The results of three methods of coupling the heat and mass transport processes are shown.

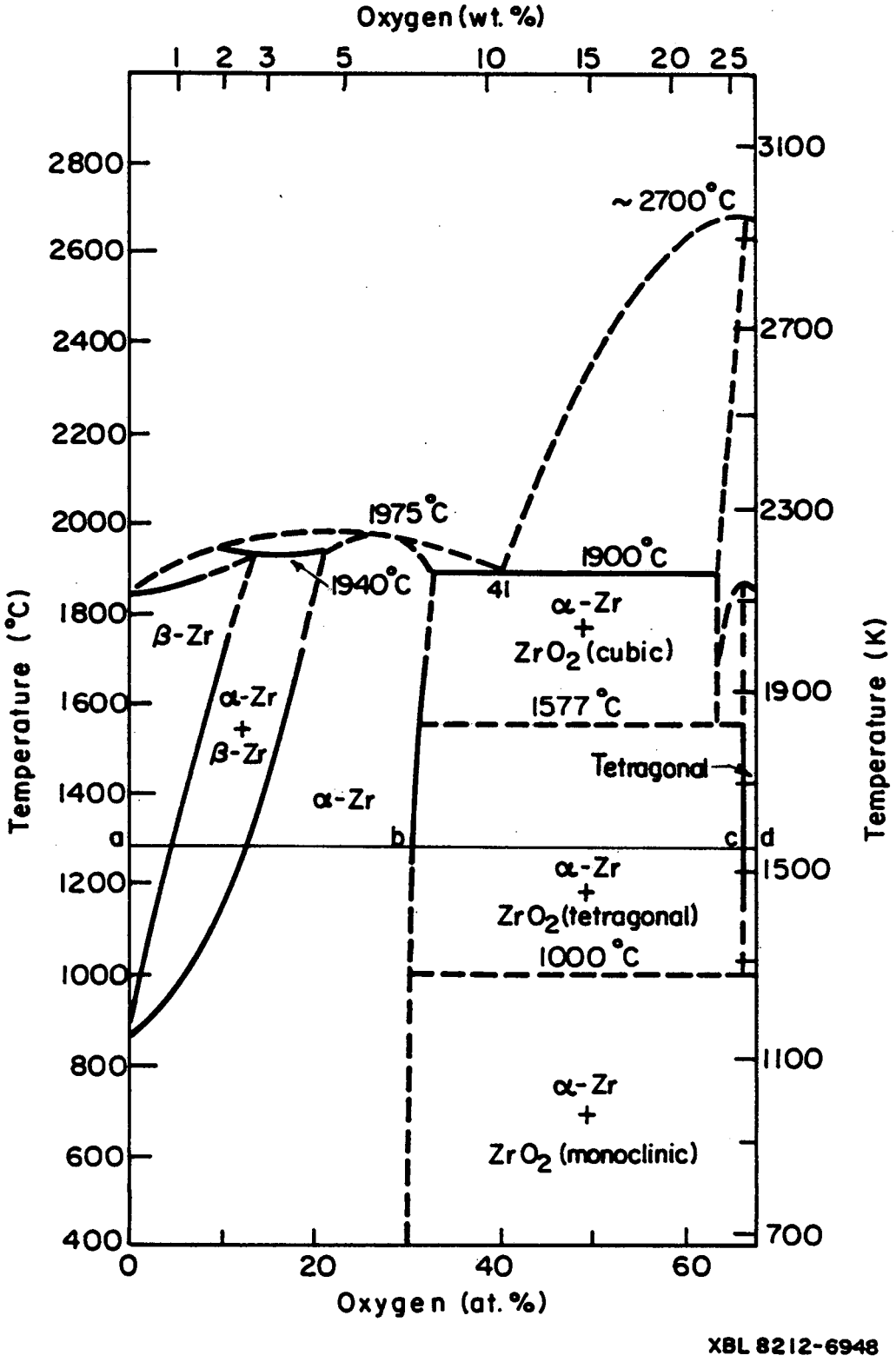
Oxygen (wt. %)
1 2 3 5 10 15 20 25
2800
2600
2400
2200
2000
1800
1600
1400
1200
1000
800
600
400
Temperature (°C)
3100
2700
2300
1900
1500
1100
700
Temperature (K)
~2700°C
1975°C
1940°C
1900°C
41
β-Zr
α-Zr
+
β-Zr
α-Zr
α-Zr
+
ZrO2 (cubic)
1577°C
Tetragonal
a
b
c
d
α-Zr
+
ZrO2 (tetragonal)
1000°C
α-Zr
+
ZrO2 (monoclinic)
0
20
40
60
Oxygen (at. %)
XBL 8212-6948

Fig. 1

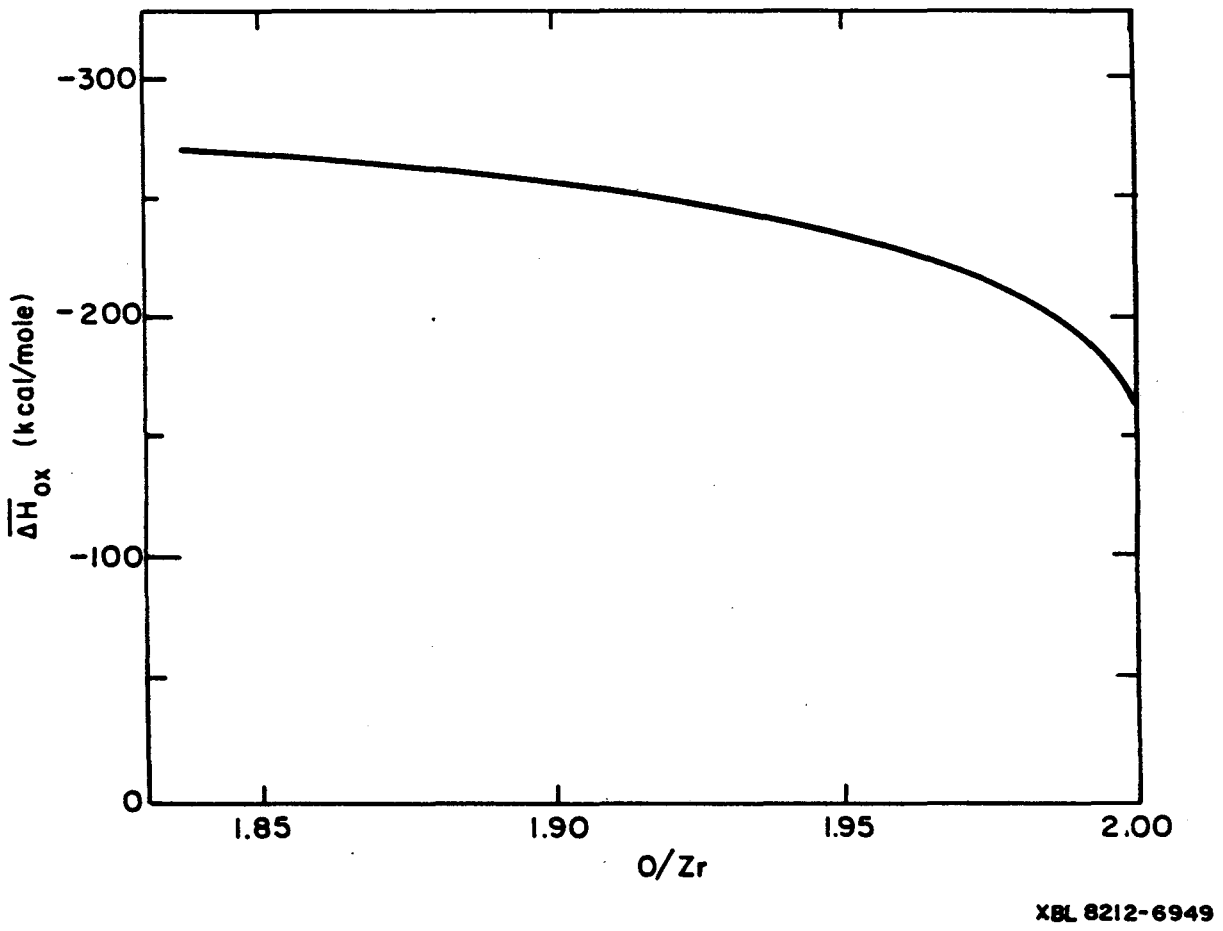
-300
-200
-100
0
$\overline{\Delta H}_{ox}$ (kcal/mole)
1.85
1.90
1.95
2.00
O/Zr
XBL 8212-6949

Fig. 2

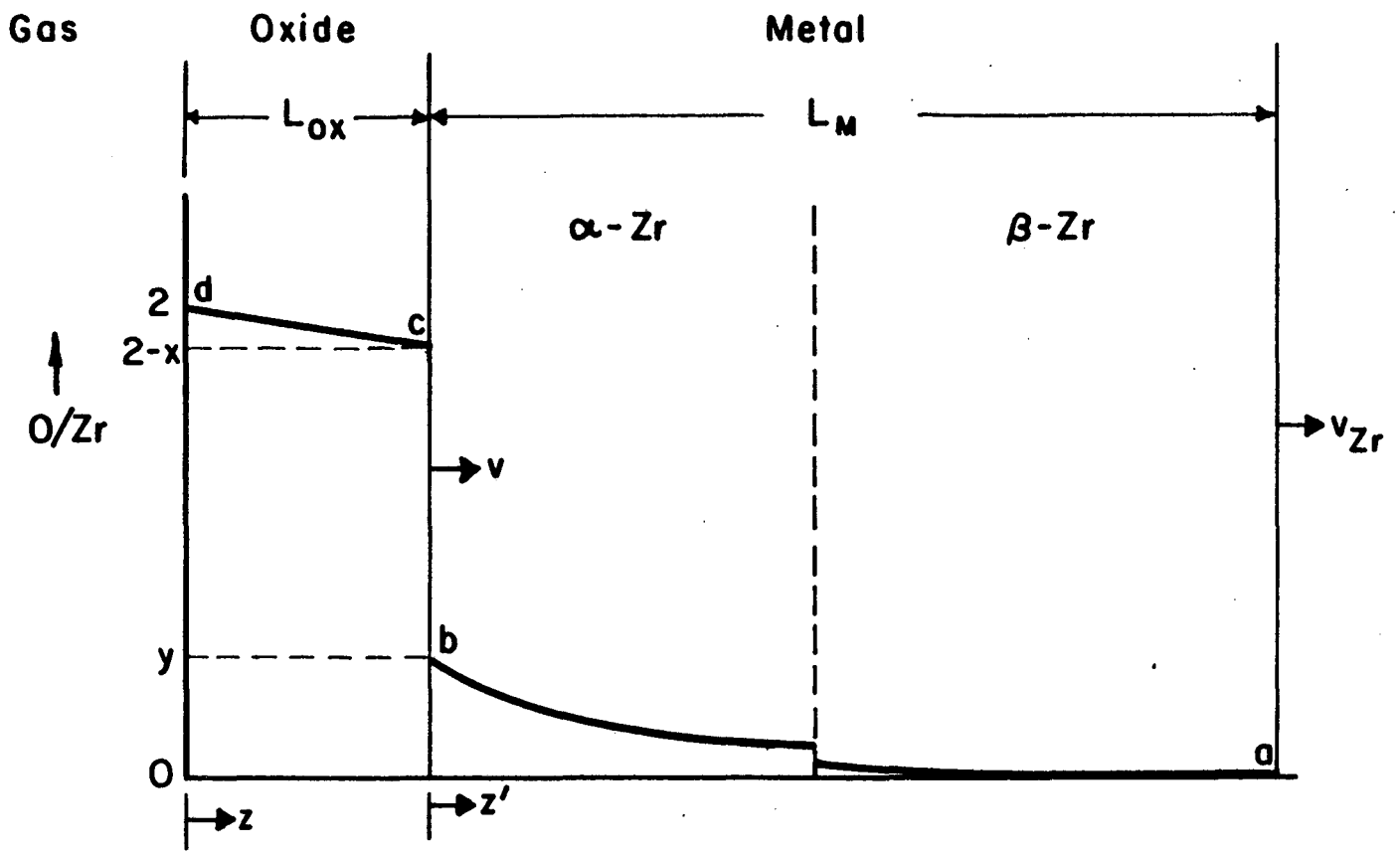


XBL 8212-6950

Fig. 3

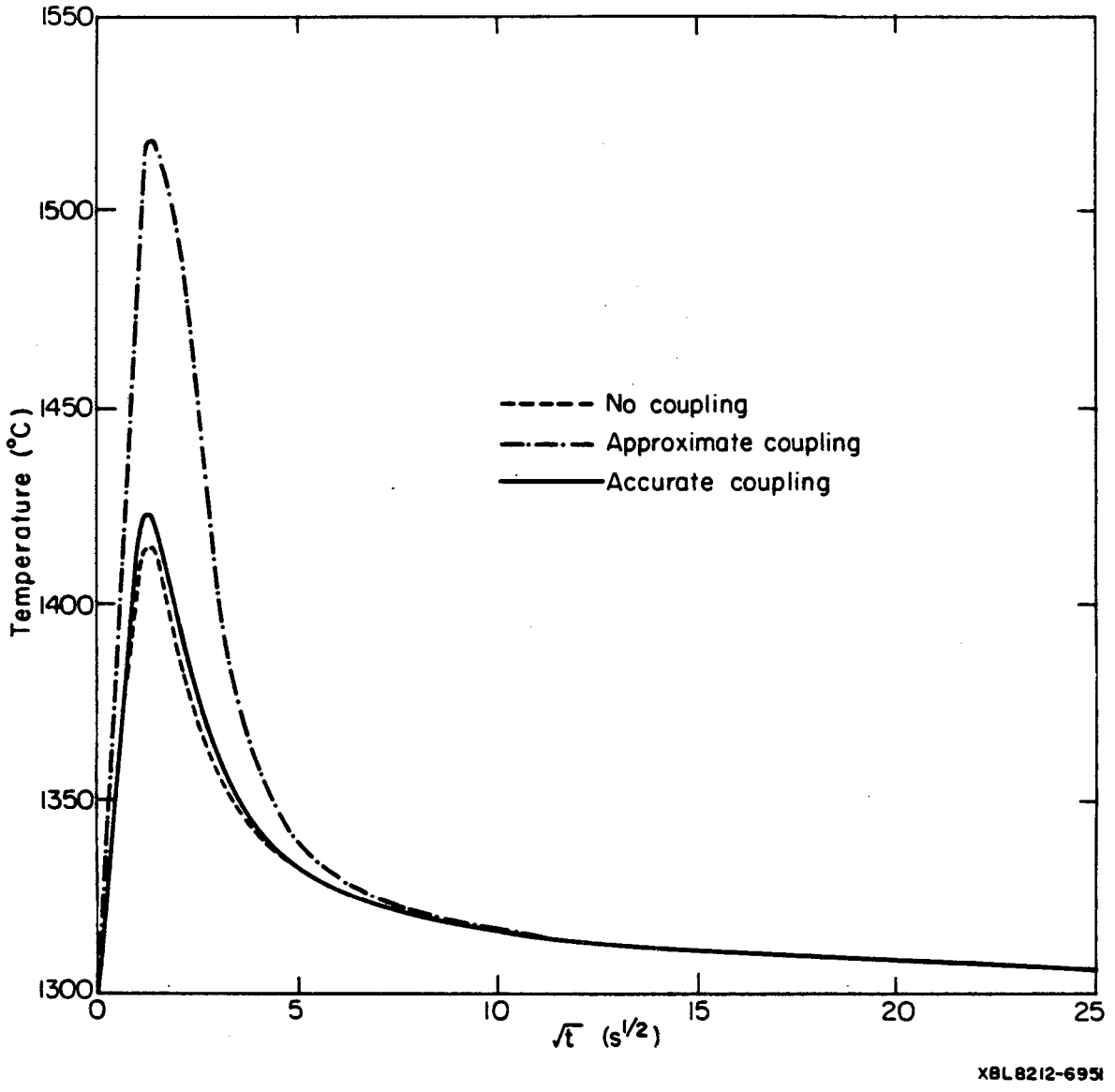
1550
1500
1450
1400
1350
1300
Temperature (°C)
0
5
10
15
20
25
√t (s^1/2)
No coupling
Approximate coupling
Accurate coupling
XBL8212-6951

Fig. 4

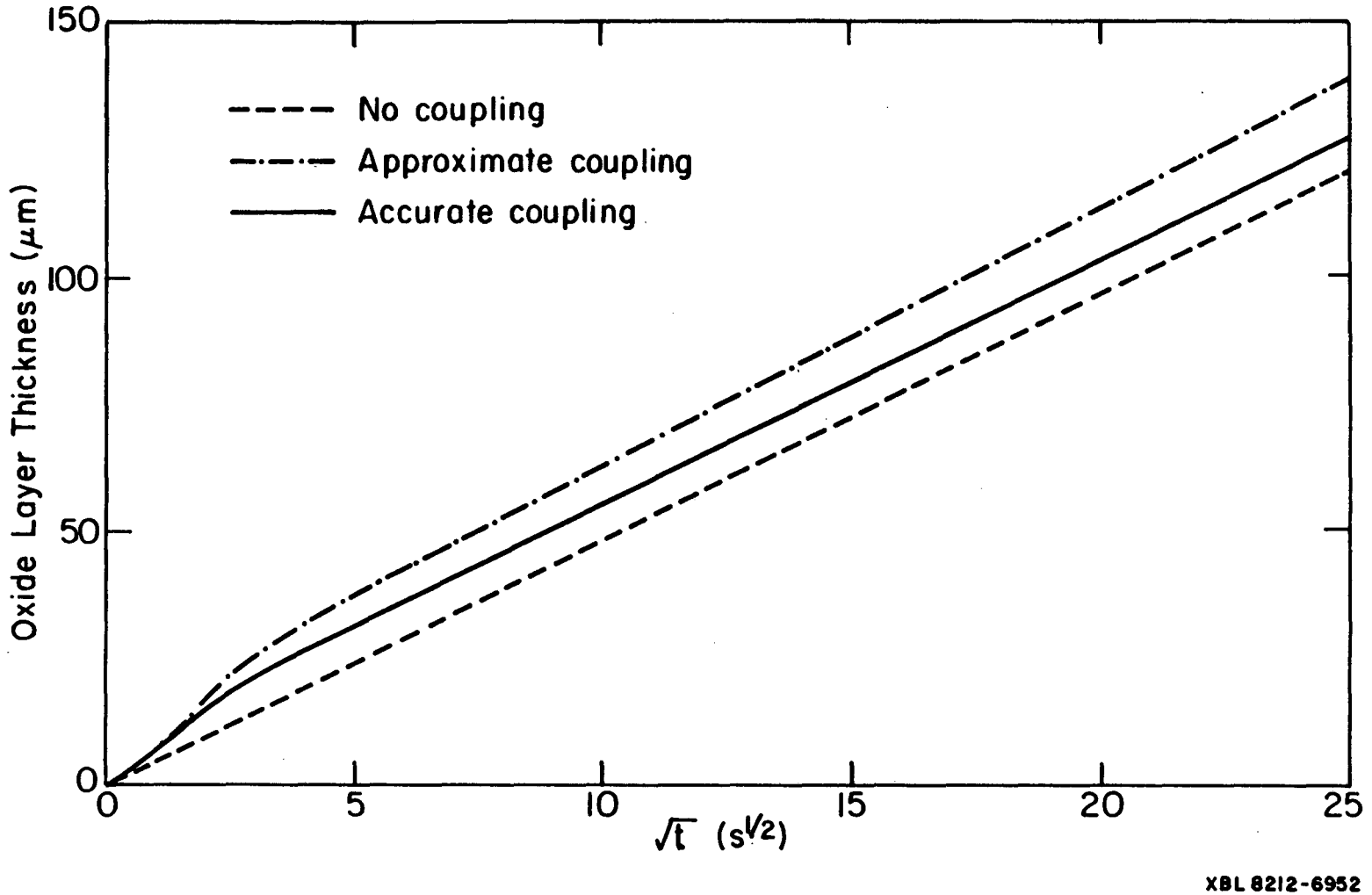
150
100
50
0
Oxide Layer Thickness (μm)
No coupling
Approximate coupling
Accurate coupling
0
5
10
15
20
25
√t (s^1/2)
XBL 8212-6952

Fig. 5

This report was done with support from the Department of Energy. Any conclusions or opinions expressed in this report represent solely those of the author(s) and not necessarily those of The Regents of the University of California, the Lawrence Berkeley Laboratory or the Department of Energy.

Reference to a company or product name does not imply approval or recommendation of the product by the University of California or the U.S. Department of Energy to the exclusion of others that may be suitable.

*TECHNICAL INFORMATION DEPARTMENT*
*LAWRENCE BERKELEY LABORATORY*
*UNIVERSITY OF CALIFORNIA*
*BERKELEY, CALIFORNIA 94720*